CHEMISTRY
A EUROPEAN JOURNAL

DOI: 10.1002/chem.200600980

Molecular Tectonics of Metal–Organic Frameworks (MOFs): A Rational Design Strategy for Unusual Mixed-Connected Network Topologies

Miao Du,*[a, b] Zhi-Hui Zhang,[a] Liang-Fu Tang,[b] Xiu-Guang Wang,[a] Xiao-Jun Zhao,[a] and Stuart R. Batten*[c]

Abstract: To systematically explore the higher-dimensional network structures with mixed connectivity, a series of two-dimensional (2D) and three-dimensional (3D) metal–organic frameworks (MOFs) with unusual (3,6)-connected net topologies are presented. These crystalline materials include $[\{[Mn(btza)_2(H_2O)_2]\cdot 2H_2O\}_n]$ (**1**), $[\{[Zn(btza)_2(H_2O)_2]\cdot 2H_2O\}_n]$ (**2**), $[\{[Cu(btza)_2]\cdot H_2O\}_n]$ (**3**), and $[\{[Cd(btza)_2]\cdot 3H_2O\}_n]$ (**4**), which have been successfully assembled through a predesigned three-connected organic component bis(1,2,4-triazol-1-yl)acetate (btza) with a variety of octahedral metal cores based on the modular synthetic methodology. The topological paradigms shown in this work cover the 2D $CdCl_2$, 3D $(4^2.6)_2(4^4.6^2.8^7.10^2)$, and pyrite (**pyr**) types. That is, when properly treated with the familiar first-row divalent metal ions, btza may perfectly furnish the coordination spheres for effective connectivity to result in diverse (3,6)-connected nets. Beyond this, a detailed analysis of network topology for all known 3D (3,6)-connected frameworks in both inorganic and inorganic–organic hybrid materials is described. Specific network connectivity of these MOFs indicates that the metal centers represent the most significant and alterable factor in structural assembly, although they show reliable and similar geometries. In this context, the combination of the distinct d^{10} Ag^I ion with btza in different solvents affords two isomorphous MOFs $[\{[Ag(btza)]\cdot glycol\}_n]$ (**5**) and $[\{[Ag(btza)]\cdot CH_3OH\}_n]$ (**6**) with a binodal 4-connected 3D $SrAl_2$ (**sra**) topology. The network structures of MOFs **1**–**3** and **5** turn out to be more complicated and interesting if one considers the hydrogen bonding between the host coordination frameworks and the intercalated solvent molecules. Furthermore, the role of the included solvents in the generation and stabilization of MOFs **1**–**6** is also investigated.

Keywords: crystal engineering · ligand design · metal–organic frameworks · network topology · topochemistry

Introduction

Metal–organic frameworks (MOFs), also known as coordination polymers,[1] represent a new class of metal–ligand coordination compounds, in which the metal centers are interconnected by organic linkers to display a variety of infinite supramolecular networks, and such useful properties as magnetic ordering, microporosity, and nonlinear optical activity.[2] Synthetic strategies for the predicted assembly of MOFs are of great importance for the desired new materials, and a modular construction or building-block methodology is proven to be efficient in the generation of premeditated frameworks, in which the connectivity information is encoded within the metal and ligand precursors.[3] However, at this stage, there are still great challenges to achieve a true rational construction of desired MOFs by predetermined molecular tectons, especially in designing new building blocks that can act as a carrier of the structural and functional information to be expressed in a specific target material.[2d]

Network topology is an important and essential aspect of the design and analysis of MOFs and also of an inherent interest in understanding the supramolecular assembly. In this

[a] Prof. M. Du, Z.-H. Zhang, X.-G. Wang, Prof. X.-J. Zhao
College of Chemistry and Life Science
Tianjin Normal University, Tianjin 300074 (China)
Fax: (+86) 22-2354-0315
E-mail: dumiao@public.tpt.tj.cn

[b] Prof. M. Du, Prof. L.-F. Tang
State Key Laboratory of Elemento-Organic Chemistry
Nankai University, Tianjin 300071 (China)

[c] Dr. S. R. Batten
School of Chemistry, Monash University
Victoria, 3800 (Australia)
Fax: (+61) 3-9905-4597
E-mail: stuart.batten@sci.monash.edu.au

Supporting information for this article is available on the WWW under http://www.chemeurj.org/ or from the author.

approach, complicated frameworks are simplified to simple node-and-connection reference nets.[4] New insights into the development of approaches for the engineering of MOFs are then possible on the basis of topological considerations.[1,3,4] Therefore, new or unusual network topologies are of considerable focus,[5] particularly those deliberately constructed from the nodes with connectivity commonly displayed by typical metal ions and organic ligands used in MOFs synthesis. Generally, they contain the required geometrical information and the directional binding modes that will facilitate the crystallization of MOFs with predesigned topologies. In particular, nodes of 3-, 4-, and 6-connectivity are of most relevance, and a variety of such uninodal network topologies have been realized so far.[4] However, there is an unfavorable lack of systematic investigation on higher-dimensional networks with mixed connectivity,[1c,4] such as (3,6)-, (4,6)-, and (4,8)-connected frameworks, which are considered to be difficult to achieve.[6] In this context, we will describe herein a successful synthetic strategy of a series of MOFs with unusual (3,6)-connected network topologies, namely $[\{[Mn(btza)_2(H_2O)_2]\cdot 2H_2O\}_n]$ (**1**), $[\{[Zn(btza)_2(H_2O)_2]\cdot 2H_2O\}_n]$ (**2**), $[\{[Cu(btza)_2]\cdot H_2O\}_n]$ (**3**), and $[\{[Cd(btza)_2]\cdot 3H_2O\}_n]$ (**4**). These MOFs are simply generated from the solution-assembly of a new potential triconnected ligand, bis(1,2,4-triazol-1-yl)acetic acid (Hbtza), with familiar octahedral metal nodes such as Mn^{II}, Zn^{II}, Cu^{II}, and Cd^{II}. Metal-directed production of two isostructural 4-connected frameworks with a $SrAl_2$ (**sra**) topology, namely $[\{[Ag(btza)]\cdot glycol\}_n]$ (**5**) and $[\{[Ag(btza)]\cdot CH_3OH\}_n]$ (**6**), is also described when using the univalent silver ion as the tetrahedral metal node (see Scheme 1 for details).

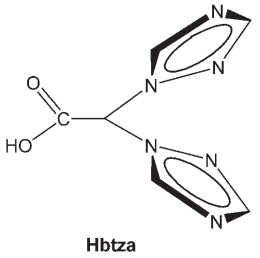

Hbtza

1: $[\{[Mn(btza)_2(H_2O)_2]\cdot 2H_2O\}_n]$

2: $[\{[Zn(btza)_2(H_2O)_2]\cdot 2H_2O\}_n]$

3: $[\{[Cu(btza)_2]\cdot H_2O\}_n]$

4: $[\{[Cd(btza)_2]\cdot 3H_2O\}_n]$

5: $[\{[Ag(btza)]\cdot glycol\}_n]$

6: $[\{[Ag(btza)]\cdot CH_3OH\}_n]$

Scheme 1.

Results and Discussion

Preparation and general characterization of MOFs 1–6: Solution-phase-directed assembly of the well-designed organic linker Hbtza with equimolar inorganic Mn^{II}, Zn^{II}, Cu^{II}, Cd^{II}, and Ag^{I} salts leads to the formation of the corresponding coordination polymers **1**–**6**. The compositions of these MOFs were determined by IR spectroscopy, single-crystal X-ray diffraction, and microanalytical techniques. The phase purities of the bulk samples were identified by powder X-ray diffraction (see Figure S1 in the Supporting Information for powder X-ray diffraction (PXRD) patterns). All complexes are stable in air and can retain their structural integrity at room temperature, thus thermogravimetric analyses were performed to determine their thermal stabilities (see Figure S2 in the Supporting Information for TGA curves). The first weight loss occurring in the range of 100–155 °C for **1**, 95–160 °C for **2**, 100–150 °C for **3**, and 40–105 °C for **4** corresponds to the release of the lattice solvates, and the host coordination frameworks of **1**–**4** remain intact upon further heating to 190, 185, 185, and 240 °C, respectively. The loss of the glycol guest in **5** is not observed before 170 °C, where the decomposition starts. Whereas for **6**, the exclusion of the captured methanol guest is detected in the temperature range of 75–165 °C, and the residual framework keeps stable up to 275 °C.

Preliminary design strategy: The design principles of MOFs **1**–**4** with mixed (3,6)-connected topologies are as follows: a) the new ligand btza has three metal binding moieties and the tripodal backbone, which will be potentially able to behave as a triconnected node; b) the carboxylate group generally makes the ligand anionic and thus eliminates the requirement for charge balance of MOFs by inorganic counter anions, which may significantly influence the assembly and thus make it untraceable for structural prediction; c) the small steric size of the triazole ring and the coordinative flexibility of the overall backbone of the ligand due to the central sp^3 carbon atom jointly help to avoid crowding at the metal sphere and thus encourage the formation of high-connectivity networks. Presumably, when btza is properly coordinated to the first-row divalent metal cations, it is able to satisfactorily complete the coordination spheres and, as a consequence, lead to the generation of the (3,6)-connected frameworks with a general formula of $M(btza)_2$.

Structural analysis and discussion: Reaction of Hbtza with $Mn(OAc)_2\cdot 4H_2O$ resulted in the crystals of $[\{[Mn(btza)_2(H_2O)_2]\cdot 2H_2O\}_n]$ (**1**). The asymmetric unit contains one half-occupied Mn^{II} atom, which lies on an inversion center, one unique btza anionic ligand, one coordinated and one intercalated water molecule. The Mn^{II} center shows an octahedral coordination (see the archived CIF file for detailed bond parameters (CCDC-607346)), coordinating to four different btza ligands through triazole nitrogen atoms (Mn–N 2.273(2) and 2.263(2) Å) in an equatorial fashion, and two *trans* axial water ligands (Mn–O 2.149(2) Å). The ligands in turn coordinate to two metal atoms, through each of its triazole pendants, and are hydrogen bonded to a water ligand on a third metal through a carboxylate group (O4–H4A···O2 (symmetry code: x, $y-1$, z), H···O/O···O distances: 1.855/2.674 Å; angle: 161°). The overall 2D sheet formed is shown in Figure 1a, with the schematic network connectivity in Figure 1b. If just the coordination links are taken into account, this structure has a simple (4,4) topology, with square-planar Mn nodes and 2-connected btza ligands. However, if the strong hydrogen bonding is also considered, then the ligands are 3-connecting and the Mn-$(H_2O)_2$ moieties act as the 6-connected nodes. Thus a (3,6)-

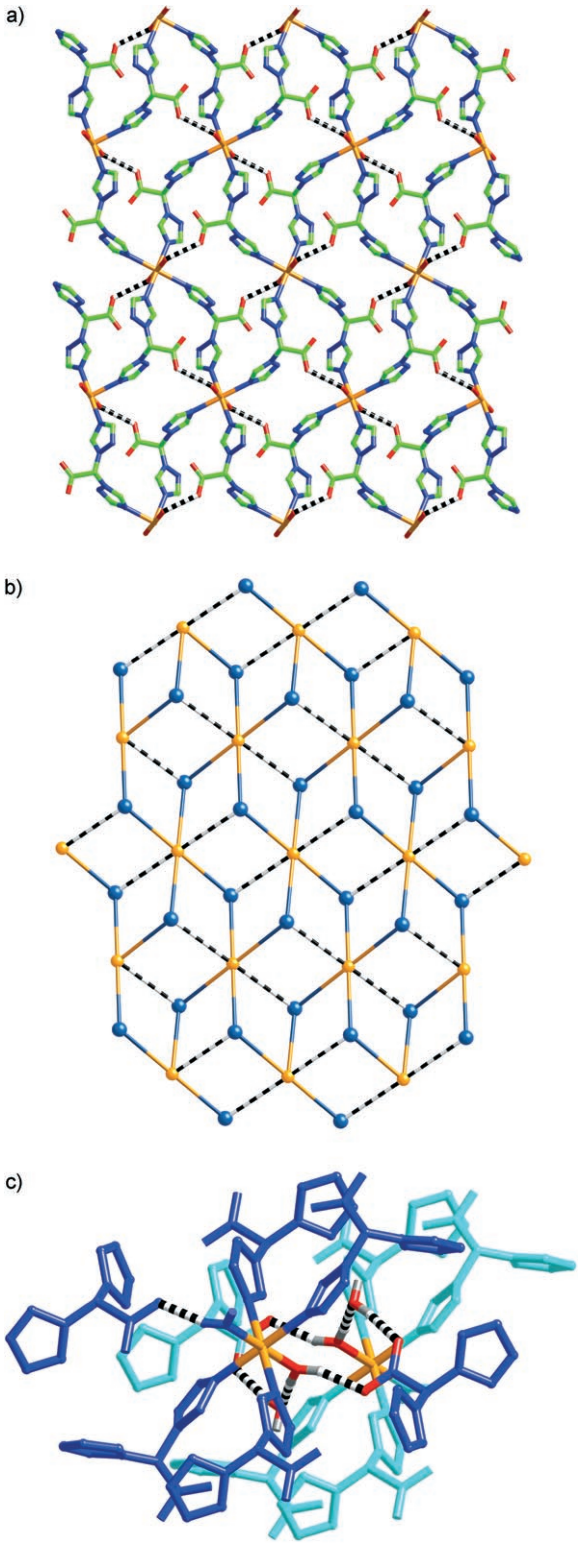

Figure 1. a) A single sheet in the structure of $[\{[Mn(btza)_2(H_2O)_2]\cdot 2H_2O\}_n]$ (**1**). Color code for atoms: metal: orange; nitrogen: blue; carbon: green; oxygen: red; hydrogen atoms and intercalated water moieties are omitted for clarity, and hydrogen bonds are depicted as the striped bonds. b) A schematic diagram of the (3,6)-connected $CdCl_2$ topology of the 2D sheet, with ligands represented by the central sp^3 carbon atoms (blue spheres). Orange spheres again represent the metal atoms. c) The bridging of two adjacent sheets through hydrogen bonds with intercalated water molecules.

connected network is formed, which has the $CdCl_2$ topology. This 2D topology with the Schläfli symbol of $(4^3)_2(4^6.6^6.8^3)$ is common for binary inorganic compounds, but quite rare for metal–organic coordination polymers, although it has been reported recently for some cyano-bridged ones.[7] The intercalated water molecules lie between the sheets and connect them through hydrogen-bonding interactions with carboxylate oxygen atoms and water ligands in adjoining sheets (O3–H3B···O1 (symmetry code: $x-1/2$, $-y+3/2$, $z+1/2$), H···O/O···O distances: 1.866/2.694 Å; angle: 169°; O4–H4B···O3 (symmetry code: $-x+1/2$, $y-1/2$, $-z+3/2$), H···O/O···O distances: 1.847/2.694 Å; angle: 174°), as depicted in Figure 1c. If these further hydrogen-bonding interactions are taken into account, then the structure of **1** turns into a very complicated 3D (3,4,6)-connected trinodal network, with the aqua ligands becoming 3-connecting nodes, btza 4-connecting nodes, and the metal centers remaining 6-connecting nodes. Accordingly, the overall Schläfli symbol becomes $(4.5.6)_2(4.5^2.6^2.7)_2(5^4.6^4.7^2.8^2.9^2.10)$.

The structure of $[\{[Zn(btza)_2(H_2O)_2]\cdot 2H_2O\}_n]$ (**2**) is essentially isostructural to **1**, with similar cell dimensions and the same gross structural features (see the archived CIF file for detailed bond parameters (CCDC-607347)). This compound, however, crystallizes in a noncentrosymmetric space group $P2_1$, whereas **1** is centrosymmetric ($P2_1/n$). A close inspection reveals that the intercalated water molecules are important in differentiating the two structures. In addition to the hydrogen bonds described above, there is also a weaker interaction between the intercalated water molecule and one triazole nitrogen atom of the btza ligand. In **1**, in which the metal ions lie on the inversion centers, these are all equivalent and rather weak (O3–H3A···N5 (symmetry code: $x-1/2$, $-y+1/2$, $z+1/2$), H···N/O···N distances: 2.428/3.104 Å; angle: 137°). In the structure of **2**, however, there are two crystallographically distinct btza ligands and intercalated water guests. One of these water molecules makes a considerably stronger hydrogen bond to the corresponding btza (O8–H8B···N8 (symmetry code: $-x+1$, $y+1/2$, $-z+1$), H···N/O···N distances: 2.166/2.967 Å; angle: 157°) than that in **1** or for the other water molecule/btza ligand pairing in **2** (O7–H7B···N5 (symmetry code: $x-1$, y, z), H···N/O···N distances: 2.607/3.073 Å; angle: 116°). As a consequence, this stronger hydrogen bond significantly twists the corresponding btza triazole ring compared with the weaker bond to the other ligand, or those in **1** (see Figure 2). These two distinct btza ligands, containing formally equivalent triazole rings in **1** now twisting differently in **2**, coordinate *trans* to each other across the metal centers, and thus the center of symmetry in **2** is lost.

Reaction of Hbtza with $Cu(OAc)_2\cdot H_2O$ gave single crystals of MOF $[\{[Cu(btza)_2]\cdot H_2O\}_n]$ (**3**). The asymmetric unit contains a half-occupied Cu atom, which lies on an inversion center, one btza ligand, and half a water molecule, which lies on a twofold axis. Each octahedral Cu^{II} ion is bound to six separated btza ligands (see Figure 3a), coordinating to four through triazole nitrogen atoms (Cu–N 2.008(2) and 2.019(2) Å), and to two through carboxylate oxygen atoms

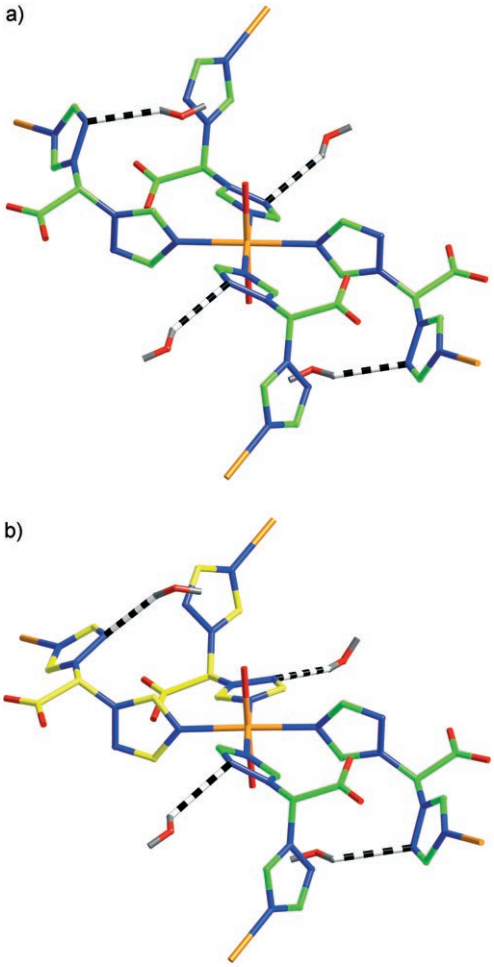

Figure 2. a) Local geometry for the centrosymmetric **1**, showing hydrogen bonding between btza triazole rings and intercalated water molecules. All btza ligands and intercalated water molecules are equivalent. b) Local geometry for the noncentrosymmetric **2**, showing hydrogen bonding between btza triazole rings and intercalated water. There are two crystallographically distinct btza ligands; those at the back and left of Figure 2b (with C atoms in yellow) interact with the intercalated O8 water much more strongly than the other type (with C atoms in green), which interact with the O7 water. This leads to a pronounced twisting of the triazole ring at the back of the metal center.

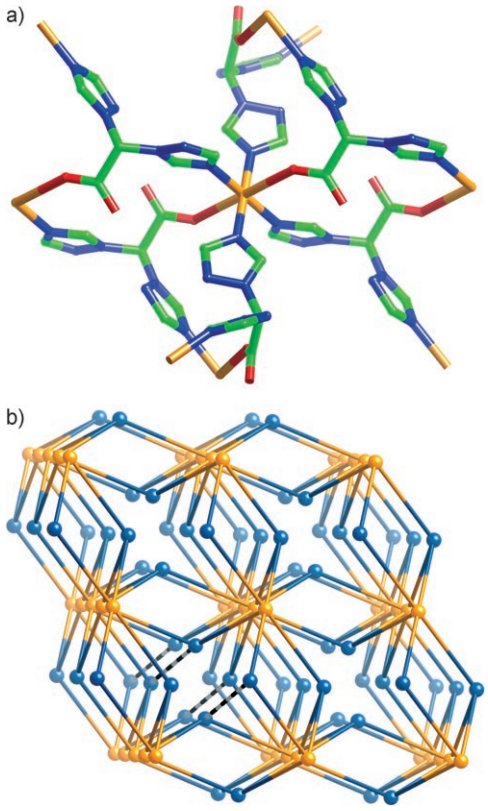

Figure 3. a) Local coordination geometry in the structure of $[\{[Cu(btza)_2]\cdot H_2O\}_n]$ (**3**). Color code for atoms, see Figure 1; included water molecules are omitted for clarity. b) A schematic view of the 3D (3,6)-connected network of $(4^2.6)_2(4^4.6^2.8^7.10^2)$ topology. For clarity, the hydrogen-bonded links (striped bonds) are shown at the bottom left only.

(Cu–O 2.429(2) Å). As expected, the Cu atom shows typical Jahn–Teller distortion, with *trans* Cu–O bonds elongated relative to the Cu–N bonds. Each ligand in turn coordinates to three Cu centers. Thus, the ligands and metals are combined to generate a 3D (3,6)-connected network (see Figure 3b) with the Schläfli symbol of $(4^2.6)_2(4^4.6^2.8^7.10^2)$. To the best of our knowledge, there is only one known example for a MOF with such a net topology,[6c] despite its apparent simplicity (with only one type of each node), and the common occurrence of 3- and 6-connecting nodes in coordination polymers. The intercalated water moiety is hydrogen bonded to the uncoordinated carboxylate oxygen atoms (O···O 2.780 Å) on two adjacent ligands, thus creating a hydrogen-bonded bridge. If this link is taken into account (as shown in Figure 3b), then the ligands become 4-connecting, and the resultant (4,6)-connected net has the Schläfli symbol $(4^2.5^3.6)_2(4^4.5^2.6^2.7^2.8^4.9)$. Also, considering two 3-connected ligands linked by the hydrogen bond as a 6-connected node, we can get a new binodal 6-connected $(4^{13}.6^2)(4^8.6^6.8)$ network.

Other (3,6)-connected 3D topologies reported for MOFs include the most frequent network, rutile (**rtl**,[8] Schläfli symbol $(4.6^2)_2(4^2.6^{10}.8^3)$),[9] as well as the **sit** net with the same Schläfli symbol $(4.6^2)_2(4^2.6^{10}.8^3)$,[10] a self-penetrating $(4.6^2)_2(4^2.6^{10}.8^3)$ network,[11] another self-penetrating net, this time with a $(4^2.6)(6^3)(4^2.6^4.8^9)$ topology,[12] the pyrite-like network (FeS_2 with the S···S bond ignored, **pyr**, Schläfli symbol $(6^3)_2(6^{12}.8^3)$),[13] the **qom** net,[14] a $(4^3)(4.6^2)(4^4.6^8.8^3)$ net,[15] a $(4.6^2)_2(4^2.6^9.8^4)$ net,[9c] a $(4.6^2)_2(4^2.6^{10}.8^3)$-c net,[1g,16] and an anatase net (**ant**, $(4^2.6)_2(4^4.6^2.8^8.10)$).[17] Recently, a hydrogen-bonded (3,6)-connected network with $(4.8^2)_2(4^2.8^{11}.10^2)$ topology has also been reported.[18] A number of other (3,6)-connected networks have been identified in inorganic materials (as far as we know not yet observed in MOFs),[8,19] including α-PbO_2 (**apo**, Schläfli symbol $(4.6^2)_2(4^2.6^9.8^4)$), ramsdellite (γ-MnO_2, $(4.6^2)(4^3)(4^4.6^8.8^3)$), brookite (**brk**, Schläfli symbol $(4.6^2)(4^2.6)(4^3.6^6.8^6)$), and PrI_2 (**spn**, Schläfli symbol $(4^3)_2(4^6.12^9)$). Overall, only eleven 3D (3,6)-connected topologies for MOFs plus a further four for inorganic materials have been documented so far. Further-

more, it should be specified that amongst these topologies, only twofold interpenetrated examples are observed for the $(4.6^2)_2(4^2.6^{10}.8^3)$-c network (MOF),[1g,16,20] as well as **spn** and γ-MnO_2 frameworks (inorganic material).[19,20]

Reaction of Hbtza with $Cd(OAc)_2{\cdot}2H_2O$ produced crystals of $[\{[Cd(btza)_2]{\cdot}3H_2O\}_n]$ (**4**). The asymmetric unit contains a half-occupied Cd^{II} ion, which lies on an inversion center, one ligand, and two unique water molecules (one of which is half-occupied). As in the previous structure, each octahedral Cd^{II} coordinates to six separate btza ligands (see Figure 4a), four through triazole nitrogen atoms (Cd–N 2.309(3) and 2.404(3) Å), and two through carboxylate oxygen atoms (Cd–O 2.387(2) Å). In turn, each ligand coordinates to three Cd^{II} centers. One of the intercalated water molecules is hydrogen bonded to both the coordinated carboxylate oxygen atom (O3–H3B···O1 (symmetry code: $-1/2$, y, $-z+3/2$), H···O/O···O distances: 2.110/2.925 Å; angle: 160°) and the other intercalated water moiety (O3–H3A···O4 (symmetry code: $-x+1/2$, $-y+1$, $z+1/2$), H···O/O···O distances: 2.227/3.075 Å; angle: 175°). An overall 3D (3,6)-connected network is again formed (see Figure 4b), however in this case the topology is that of the pyrite net (**pyr**), and as stated in the above topology analysis, only a small number of structures with this topology have been reported hitherto.[13]

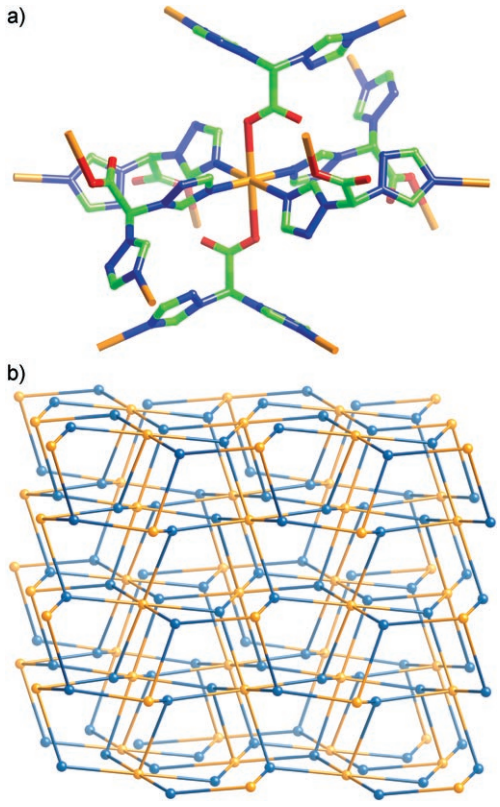

Figure 4. (a) Local coordination geometry in the structure of $[\{[Cd(btza)_2]{\cdot}3H_2O\}_n]$ (**4**). Color code for atoms, see Figure 1; included water molecules are omitted for clarity. b) A schematic view of the pyrite-like (**pyr**) 3D (3,6)-connected network.

For MOFs **1**–**4**, assembling a triangular building block Hbtza with octahedral metals realizes the predesigned (3,6)-mixed connectivity networks, which, however, display diverse topologies that cannot be accurately forecasted at this stage. In particular, for **3** and **4**, the ligand and metal nodes have apparently similar binding modes, but distinct propagation in the crystal packing results in the formation of different 3D frameworks. However, the subtle differences in the binding modes of the ligand in **1**–**4** can be seen in Figures 5a–e. In all these structures the uncoordinated 2-position ni-

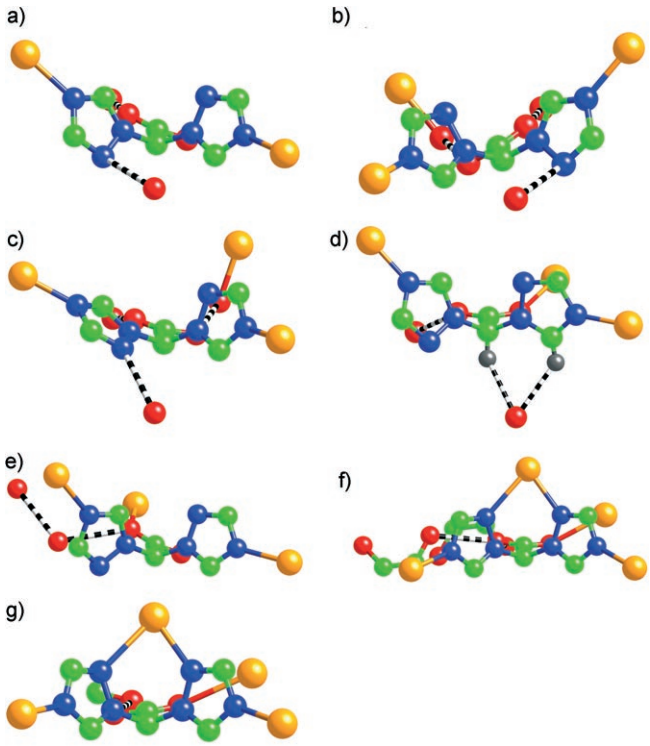

Figure 5. Ligand geometries viewed almost directly down the central C–C bond. Color code for atoms, see Figure 1: a) **1**; b) and c) **2**; d) **3**; e) **4**; f) **5**, and g) **6**.

trogen atoms on the two triazole rings point in opposite directions. And thus the most significant differences between the structures are not the ligand geometries (apart from very small differences in the twist angles of the carboxylate group), but the relative disposition of the groups bound to the carboxylate oxygen atoms (either through hydrogen or coordinative bonding). Notably, even the disposition of the metal centers bonded to the triazole rings remains the same in these structures.

Nonetheless, from a crystal engineering point of view, the most significant and alterable parameter in the crystallization processes of **1**–**4** is the metal ion, which plays a key role in the final topology formation although they have very reliable and similar geometrical preferences. This observation motivates us to further explore the metal-directed assembly of MOFs with btza by using the adaptable silver(I) center, which can afford a variety of coordination geometries, but

mainly display the linear and tetrahedral ones.[21] In the structure of [{[Ag(btza)]·glycol}$_n$] (**5**), the asymmetric unit contains one metal ion, one ligand anion, and one glycol guest molecule. Each Ag atom is coordinated to four ligands (see Figure 6a); one ligand coordinates in a bidentate fashion through two triazole nitrogen atoms (Ag–N 2.348(3) and 2.680(3) Å), and thus the metal is pentacoordinated. It coordinates to two other ligands through triazole nitrogen atoms (Ag–N 2.298(3) and 2.319(3) Å), and one other through a carboxylate oxygen atom (Ag–O 2.580(3) Å). The ligands are thus pentadentate, but coordinate to only four silver atoms. For comparison, the ligand geometry is depicted in Figure 5f viewed from the same angle as the other four structures; the most notable feature is the fact that the 2-position nitrogen atoms of two triazole rings are directed to the same side of the ligand (and indeed chelate to a single Ag center). The intercalated glycol moieties are hydrogen-bonded in pairs to the uncoordinated carboxylate oxygen atoms of the adjoining molecules (O3–H3A···O1 (symmetry code: $-x$, $-y+2$, $-z+1$), H···O/O···O distances: 1.956/2.769 Å; angle: 171°; O4–H4···O1 (symmetry code: $x+1$, y, $z+1$), H···O/O···O distances: 1.951/2.757 Å; angle: 167°). However, if one considers only the coordination bonds, both the Ag atom and the ligand act as 4-connecting nodes. The overall 3D network is depicted in Figure 6b, and the topology is $SrAl_2$ (**sra**). This topology is unusual in comparison to the more commonly observed 4-connected diamond (**dia**) topology—a recent systematic survey found 233 diamondoid nets, but only 31 nets with a $SrAl_2$ (**sra**) topology.[4] The hydrogen-bonding connections through the intercalated ethylene glycol molecules further reinforce the 3D network, as shown for one of the channels in Figure 6b. If one takes into account the hydrogen bonded links, a new (4,5)-connected network is generated (the ligands become 5-connecting in this condition), which has a $(4^2.6^3.7)(4^2.6^5.7^2.8)$ topology.

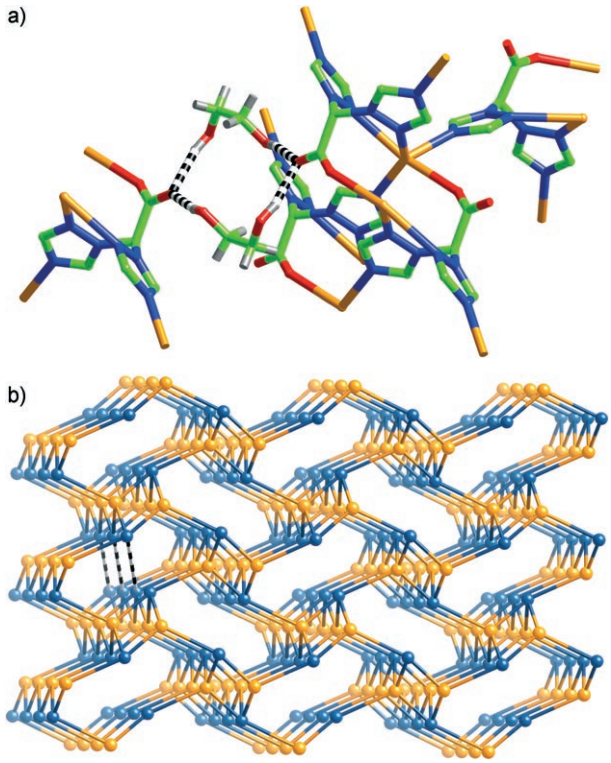

Figure 6. a) Local coordination geometry and hydrogen bonding (striped bonds) to the intercalated glycol molecules in the structure of [{[Ag(btza)]·glycol}$_n$] (**5**). Color code for atom, see Figure 1. b) A schematic view of the 3D 4-connected network with the $SrAl_2$ (**sra**) topology. For clarity, the reinforcing hydrogen bonding is shown schematically in only one channel.

The structure of [{[Ag(btza)]·CH_3OH}$_n$] (**6**) is isomorphous to **5** (see the archived CIF file for detailed bond parameters (CCDC-607350) and Figure 5g for ligand geometry). However, because the methanol guests occupy the similar positions in the lattice to the glycol molecules in **5**, they each are hydrogen bonded to only one carboxylate oxygen atom. In turn, each uncoordinated carboxylate oxygen atom forms hydrogen bonds with only one methanol molecule, and thus there are no hydrogen-bonded bridges across the $SrAl_2$ (**sra**) network in this case.

Role of solvent guests in the generation and stabilization of MOFs: From the above topological analysis of the network structures, we could easily see that the intercalated solvent molecules play a significant role in the construction of these architectures. Observing the structures reveals that the whole supramolecular networks of **1**–**3** and **5** appear to be more complicated if we consider the hydrogen-bonded interactions between the host frameworks and the solvate guests beyond the coordinative forces. For examples, a trinodal (3,4,6)-connected 3D network is reformed for **1** and **2**, a (4,6)-connected net for **3**, and a (4,5)-connected net for **5**, in which the solvates act as the hydrogen-bonding bridges to further modify their network structures. In this context, one may wonder what the nature of the host framework is, after the removal of the clathrate solvates. Thus, a fresh sample of **1**–**4** was placed in a quartz tube and dried under a high vacuum at 170 °C for 4 h to exclude the water molecules, according to the results of the TGA experiments. The composition of the solid products seems to be the dehydrates of **1**–**4**, which is evidently testified by the weight loss of the samples (7.09 % for **1**, 6.65 % for **2**, 4.15 % for **3**, and 9.90 % for **4**) and microanalysis. However, the powder X-ray diffraction (PXRD) patterns of these evacuated solids (see Figure S3 in the Supporting Information) suggest that only the host frameworks of **1** and **4** may be retained, and a framework collapse or even (partial) loss of the crystallographic periodicity occurs for **2** and **3**. As for MOFs **5** and **6** with different glycol or methanol guests, TGA experiment confirms that glycol loss is extremely difficult and the guest is not released in a dividing weight-loss step before decomposition. This may be ascribed to the higher boiling point of glycol as well as the formation of strong hydrogen bonding. A similar heating treatment of **5** and **6** at 140 °C for 4 h indicates a weight loss of 10.15 % for **5** and 9.47 % for **6**. The mass loss

of **5** under such a condition is understandable although it is not fully consistent with the content of the total glycol. The PXRD patterns of the resultant frameworks are essentially identical to those of the intact crystalline materials for both cases. These results also suggest that the solvates are important in reinforcing these structures, especially a template role in the formation of MOFs **2** and **3**.

Conclusions and Perspectives

In summary, by taking advantage of the well-defined coordination geometries of metal nodes and the organic bridging ligand bis(1,2,4-triazol-1-yl)acetate as suitable linkers, a series of unusual (3,6)-connected topological paradigms including 2D $CdCl_2$, 3D $(4^2.6)_2(4^4.6^2.8^7.10^2)$, and pyrite (**pyr**), as well as a pair of 4-connected $SrAl_2$ (**sra**) nets (or a binodal (4,5)-connected net for **5**) have been artificially reproduced in coordination polymers **1**–**6**. Moreover, network structure analysis for all known 3D (3,6)-connected topologies in both MOFs and inorganic materials has also been performed to further understand this issue. The design and synthetic concept described here offers an exciting avenue of research on metal–organic frameworks with mixed-connected network topologies, and we anticipate it to be a general and feasible strategy for other rational combinations of different connectivities within a net structure, which may promise great advance in crystal engineering. This work also suggests that such a type of anionic modular component (e.g., btza herein) is a useful building block in constructing a framework with the desired topology, which may open up new opportunities for further exploration of coordination polymer chemistry.

Experimental Section

Materials and physical measurements: With the exception of the new ligand bis(1,2,4-triazol-1-yl)acetic acid (Hbtza) which was synthesized as described below, all starting materials and solvents were obtained commercially and used as received. Fourier transform (FT)IR spectra (KBr pellets) were taken by using an AVATAR-370 (Nicolet) spectrometer. Elemental (carbon, hydrogen, and nitrogen) analyses were performed on a CE-440 (Leemanlabs) analyzer. The melting point was recorded on a WRS-1B digital thermal apparatus without correction. NMR spectra (^1H and ^{13}C) were recorded on a Bruker AV300 spectrometer, and the chemical shifts were reported in ppm with respect to reference standards (internal $SiMe_4$). Powder X-ray diffraction (PXRD) patterns were recorded on a Rigaku RU200 diffractometer at 60 kV, 300 mA for $Cu_{K\alpha}$ radiation ($\lambda =$ 1.5406 Å), with a scan speed of 2° min^{-1} and a step size of 0.02° in 2θ. The calculated PXRD patterns were produced by using the PowderCell program and single-crystal diffraction data. Thermogravimetric analysis (TGA) experiments were carried out by using a Dupont thermal analyzer in the temperature range of 25–700 °C under nitrogen atmosphere at a heating rate of 10 °C min^{-1}.

Synthesis of the ligand bis(1,2,4-triazol-1-yl)acetic acid (Hbtza): Dichloroacetyl chloride (3.9 mL, 40 mmol), 1,2,4-triazole (8.3 g, 120 mmol), KOH (8.2 g, 146 mmol), K_2CO_3 (20.9 g, 151 mmol), and benzyltriethylammonium chloride (1.0 g, 4.4 mmol) were dissolved in THF (200 mL). The mixture was stirred and refluxed for 10 h. After cooling to RT, the solvents were removed under reduced pressure. The residue was redissolved in water (150 mL) and acidified to a pH value of 7 with HCl (6 mol L^{-1}). The water solution was extracted with diethyl ether (3×150 mL), and then the organic phase was discarded to remove the excess triazole. The water phase was further acidified to a pH value of 1 and extracted again three times with a solvent mixture of diethyl ether/THF (120/40 mL). The organic layers were combined and dried by anhydrous Na_2SO_4. After the solvents had been removed under reduced pressure, the target product was obtained as a white solid (1.9 g), which was recrystallized from hot acetone/THF to afford a white microcrystalline solid in a yield of 25% (m.p. 175.4–177.8 °C). ^1H NMR (D_2O): $\delta = 8.91$ (s, 2H; triazol), 8.14 (s, 2H; triazol), 7.51 ppm (s, 1H; −CH); ^{13}C NMR (D_2O): $\delta = 165.95$ (C=O), 149.99, 145.36 (3- or 5-position carbon of triazole), 72.19 ppm (−CH); IR: $\tilde{\nu} = 3141$ (s), 3118 (s), 2992 (m), 1709 (s), 1565 (w), 1504 (m), 1422 (m), 1363 (m), 1280 (m), 1186 (m), 1126 (m), 1010 (s), 878 (m), 831 (s), 786 (w), 747 (m), 682 (w), 653 (w), 628 cm^{-1} (m); elemental analysis calcd (%) for $C_6H_6N_6O_2$: C 37.11, H 3.09, N 43.30; found: C 36.98, H 3.15, N 43.37.

Preparation of MOFs 1–6:

[{[Mn(btza)$_2$(H$_2$O)$_2$]·2H$_2$O}$_n$] (1): Hbtza (58 mg, 0.3 mmol) and Mn(OAc)$_2$·4H$_2$O (74 mg, 0.3 mmol) were mixed and dissolved in a H_2O/CH_3OH solution (v/v = 1:1, 10 mL) with stirring for 30 min. Then the solution was filtered and left to stand under ambient conditions. Upon slow evaporation of the solvents, colorless prismatic crystals suitable for X-ray analysis were produced over two weeks in a yield of 52% (based on Hbtza). IR: $\tilde{\nu} = 3428$ (b), 3115 (m), 2980 (m), 2851 (m), 2501 (w), 1665 (vs), 1593 (vs), 1517 (s), 1447 (m), 1362 (vs), 1278 (s), 1239 (w), 1207 (m), 1130 (vs), 1023 (m), 981 (s), 905 (m), 879 (m), 835 (s), 794 (m), 753 (s), 673 (s), 649 (m), 613 (w), 454 cm^{-1} (w); elemental analysis calcd (%) for $C_{12}H_{18}MnN_{12}O_8$: C 28.08, H 3.53, N 32.75; found: C 28.25, H 3.87, N 32.47.

[{[Zn(btza)$_2$(H$_2$O)$_2$]·2H$_2$O}$_n$] (2): A similar synthetic procedure was applied as that for **1**, except that Zn(OAc)$_2$·2H$_2$O was used instead of Mn(OAc)$_2$·4H$_2$O. Colourless brick-shaped crystals were collected in 62% yield (based on Hbtza) after a period of 1 month. IR: $\tilde{\nu} = 3144$ (b), 2960 (m), 1662 (s), 1521 (m), 1447 (m), 1371 (s), 1314 (w), 1286 (m), 1204 (m), 1130 (s), 1024 (w), 986 (m), 837 (m), 762 (m), 671 (m), 457 cm^{-1} (w); elemental analysis calcd (%) for $C_{12}H_{18}N_{12}O_8Zn$: C 27.52, H 3.46, N 32.09; found: C 27.25, H 3.25, N 31.84.

[{[Cu(btza)$_2$]·H$_2$O}$_n$] (3): Hbtza (19 mg, 0.1 mmol) was dissolved in a hot H_2O/DMF solution (v/v = 1:1, 6 mL), and a C_2H_5OH solution of triethylamine was added with stirring to adjust the pH value to approximately 8. The resulting solution was placed in a straight glass tube, to which a methanol (5 mL) solution of Cu(OAc)$_2$·H$_2$O (20 mg, 0.1 mmol) was carefully layered on. Blue prismatic crystals were observed on the tube wall over a period of one week. Yield: 56% (based on Hbtza). IR: $\tilde{\nu} = 3435$ (br), 3103 (m), 3038 (w), 2976 (m), 1660 (vs), 1529 (s), 1458 (m), 1359 (s), 1299 (m), 1274 (s), 1216 (m), 1126 (vs), 1026 (m), 1002 (m), 927 (w), 892 (m), 831 (s), 756 (s), 673 (s), 645 (w), 589 cm^{-1} (m); elemental analysis calcd (%) for $C_{12}H_{12}CuN_{12}O_5$: C 30.81, H 2.59, N 35.93; found: C 30.59, H 2.56, N 35.87.

[{[Cd(btza)$_2$]·3H$_2$O}$_n$] (4): A similar synthetic procedure as that for **3** was applied, except that Cu(OAc)$_2$·H$_2$O was replaced by Cd(OAc)$_2$·2H$_2$O (27 mg, 0.1 mmol), giving colorless lamellar crystals of **4** after one week in 89% yield (based on Hbtza). IR: $\tilde{\nu} = 3464$ (b), 3140 (m), 2986 (m), 1656 (vs), 1515 (s), 1445 (m), 1366 (s), 1280 (s), 1188 (s), 1127 (vs), 1020 (s), 980 (s), 909 (w), 887 (m), 836 (s), 766 (s), 672 (s), 648 (m), 608 cm^{-1} (m); elemental analysis calcd (%) for $C_{12}H_{16}CdN_{12}O_7$: C 26.08, H 2.92, N 30.41; found: C 26.06, H 2.56, N 30.38.

[{[Ag(btza)]·glycol}$_n$] (5): A CH_3CN (5 mL) solution of $AgBF_4$·4CH_3CN (36 mg, 0.1 mmol) was carefully layered onto a buffer layer of glycol (2 mL), below which a solution of Hbtza (19 mg, 0.1 mmol) in $CHCl_3$/DMF (v/v = 2:1, 6 mL) was placed in a straight glass tube. The mixture system was allowed to stand at room temperature in the dark and colorless lamellar crystals were observed on the tube wall over a period of two weeks. Yield: 63%. IR: $\tilde{\nu} = 3398$ (br), 3117 (w), 2951 (w), 2864 (w), 1662 (vs), 1510 (s), 1431 (m), 1368 (s), 1279 (s), 1203 (m), 1137 (s), 1086 (m), 1050 (w), 1019 (m), 964 (w), 882 (m), 833 (m), 761 (m), 678 cm^{-1}

Table 1. Crystal data and structural refinement summary for MOFs **1**–**6**.

	1	**2**	**3**	**4**	**5**	**6**
empirical formula	$C_{12}H_{18}MnN_{12}O_8$	$C_{12}H_{18}ZnN_{12}O_8$	$C_{12}H_{12}CuN_{12}O_5$	$C_{12}H_{16}CdN_{12}O_7$	$C_8H_{11}AgN_6O_4$	$C_7H_9AgN_6O_3$
M_r	513.32	523.75	467.88	552.77	363.10	333.07
crystal system	monoclinic	monoclinic	monoclinic	orthorhombic	monoclinic	monoclinic
space group	$P2_1/n$	$P2_1$	$C2/c$	$Pbca$	$P2_1/c$	$P2_1/c$
a [Å]	7.7344(6)	7.681(1)	10.127(1)	10.094(1)	6.612(1)	6.6194(4)
b [Å]	8.9675(7)	8.898(1)	13.037(2)	12.511(1)	10.960(2)	9.9578(6)
c [Å]	15.146(1)	15.151(2)	13.304(2)	15.172(2)	16.952(3)	16.5323(1)
β [°]	93.174(1)	90.678(2)	105.085(2)	90	100.340(2)	99.137(1)
V [Å^3]	1048.9(1)	1035.4(2)	1695.9(4)	1915.9(4)	1208.5(4)	1075.9(1)
Z	2	2	4	4	4	4
ρ_{calcd} [g cm^{-3}]	1.625	1.680	1.832	1.916	1.996	2.056
μ [mm^{-1}]	0.699	1.256	1.350	1.209	1.690	1.882
F(000)	526	536	948	1104	720	656
total/independent reflns	5525/1840	5622/3584	4777/1490	10217/1677	6425/2124	5661/1897
parameters	151	298	138	151	174	146
R_{int}	0.0346	0.0145	0.0189	0.0316	0.0225	0.0136
R[a], R_w[b]	0.0362, 0.1039	0.0310, 0.0744	0.0265, 0.0748	0.0281, 0.0942	0.0317, 0.0917	0.0240, 0.0615
GOF[c]	1.078	1.036	1.086	1.026	1.087	1.087
residuals [e Å^{-3}]	0.738, −0.439	0.215, −0.193	0.401, −0.215	0.555, −0.929	0.752, −0.592	0.776, −0.813

[a] $R=\Sigma||F_o|-|F_c||/\Sigma|F_o|$. [b] $R_w=[\Sigma[w(F_o^2-F_c^2)^2]/\Sigma w(F_o^2)^2]^{1/2}$. [c] GOF$=\{\Sigma[w(F_o^2-F_c^2)^2]/(n-p)\}^{1/2}$.

(m); elemental analysis calcd (%) for $C_8H_{11}AgN_6O_4$: C 26.46, H 3.05, N 23.15; found: C 26.78, H 2.81, N 23.25.

[{[Ag(btza)]·CH$_3$OH}$_n$] (6): A solution of $AgNO_3$ (17 mg, 0.1 mmol) in CH_3OH (5 mL) was carefully layered onto a H_2O/CH_3CN solution (v/v = 1:1, 6 mL) of Hbtza (39 mg, 0.2 mmol) in a straight glass tube. The mixture was allowed to stand under ambient conditions in the dark and colorless block crystals were observed on the tube wall over a period of two weeks in a yield of 68%. IR: $\tilde{\nu}$ = 3410 (m), 3114 (m), 2348 (w), 2257 (m), 2214 (w), 2148 (s), 1659 (s), 1508 (m), 1430 (m), 1367 (s), 1327 (w), 1277 (m), 1200 (m), 1136 (m), 1058 (w), 1016 (w), 961 (w), 832 (w), 760 (m), 677 (m), 587 (w), 524 (w), 485 (w), 420 cm^{-1} (w); elemental analysis calcd (%) for $C_{14}H_8Ag_2N_{12}O_6$: C 25.63, H 1.23, N 25.62; found: C 25.45, H 1.25, N 25.47.

X-ray data collection and structure determinations: X-ray single-crystal diffraction data for MOFs **1**–**6** were collected by using a Bruker Apex II CCD diffractometer at 293(2) K with $Mo_{K\alpha}$ radiation (λ = 0.71073 Å) by ω scan mode. There was no evidence of crystal decay during data collection in all cases. Semiempirical absorption corrections were applied by using SADABS and the program SAINT was used for integration of the diffraction profiles.[22] All structures were solved by direct methods by using the SHELXS program of the SHELXTL package and refined with SHELXL[23] by the full-matrix least-squares methods with anisotropic thermal parameters for all non-hydrogen atoms on F^2. Hydrogen atoms bonded to C atoms were placed geometrically and partial solvated hydrogen atoms were first located in difference Fourier maps and then fixed in the calculated sites. Further details for crystallographic data and structural analysis are listed in Table 1. Figures were generated by using CrystalMaker.[24]

CCDC-607346 (**1**), CCDC-607347 (**2**), CCDC-607348 (**3**), CCDC-607349 (**4**), CCDC-607350 (**5**), and CCDC-607351 (**6**) contain the supplementary crystallographic data for this paper. These data can be obtained free of charge from the Cambridge Crystallographic Data Centre via www.ccdc.cam.ac.uk/data_request/cif.

Acknowledgements

This work was financially supported by the National Natural Science Foundation of China (20401012), the National Fundamental Research Project of China (2005CCA01200), the Key Project of Chinese Ministry of Education (205008), and the Australian Research Council. One of the referees is greatly acknowledged for the invaluable comments on network topology.

[1] a) B. F. Hoskins, R. Robson, *J. Am. Chem. Soc.* **1990**, *112*, 1546–1554; b) S. R. Batten, R. Robson, *Angew. Chem.* **1998**, *110*, 1558–1595; *Angew. Chem. Int. Ed.* **1998**, *37*, 1460–1494; c) M. O'Keeffe, M. Eddaoudi, H. Li, T. Reineke, O. M. Yaghi, *J. Solid State Chem.* **2000**, *152*, 3–20; d) S. R. Batten, *Curr. Opin. Solid State Mater. Sci.* **2001**, *5*, 107–114; e) B. Moulton, M. J. Zaworotko, *Chem. Rev.* **2001**, *101*, 1629–1658; f) L. Carlucci, G. Ciani, D. M. Proserpio, *Coord. Chem. Rev.* **2003**, *246*, 247–289; g) V. A. Blatov, L. Carlucci, G. Ciani, D. M. Proserpio, *CrystEngComm* **2004**, *6*, 378–395.

[2] a) O. R. Evans, W. Lin, *Acc. Chem. Res.* **2002**, *35*, 511–522; b) C. Janiak, *Dalton Trans.* **2003**, 2781–2804; c) S. L. James, *Chem. Soc. Rev.* **2003**, *32*, 276–288; d) O. M. Yaghi, M. O'Keeffe, N. W. Ockwig, H. K. Chae, M. Eddaoudi, J. Kim, *Nature* **2003**, *423*, 705–714; e) L. Brammer, *Chem. Soc. Rev.* **2004**, *33*, 476–489; f) S. Kitagawa, R. Kitaura, S. Noro, *Angew. Chem.* **2004**, *116*, 2388–2430; *Angew. Chem. Int. Ed.* **2004**, *43*, 2334–2375; g) J. L. C. Rowsell, O. M. Yaghi, *Microporous Mesoporous Mater.* **2004**, *73*, 3–14; h) D. Bradshaw, J. B. Claridge, E. J. Cussen, T. J. Prior, M. J. Rosseinsky, *Acc. Chem. Res.* **2005**, *38*, 273–282; i) E. Coronado, D. Gatteschi, *J. Mater. Chem.* **2006**, *16*, 2513–2515.

[3] a) R. Robson, *J. Chem. Soc. Dalton Trans.* **2000**, 3735–3744; b) R. J. Hill, D.-L. Long, N. R. Champness, P. Hubberstey, M. Schröder, *Acc. Chem. Res.* **2005**, *38*, 337–350.

[4] N. W. Ockwig, O. Delgado-Friedrichs, M. O'Keeffe, O. M. Yaghi, *Acc. Chem. Res.* **2005**, *38*, 176–182.

[5] a) D. L. Long, A. J. Blake, N. R. Champness, C. Wilson, M. Schröder, *J. Am. Chem. Soc.* **2001**, *123*, 3401–3402; b) B. Moulton, J. J. Lu, M. J. Zaworotko, *J. Am. Chem. Soc.* **2001**, *123*, 9224–9225; c) M.-L. Tong, X.-M. Chen, S. R. Batten, *J. Am. Chem. Soc.* **2003**, *125*, 16170–16171; d) L. Carlucci, G. Ciani, D. M. Proserpio, F. Porta, *Angew. Chem.* **2003**, *115*, 331–336; *Angew. Chem. Int. Ed.* **2003**, *42*, 317–322; e) D. L. Long, R. J. Hill, A. J. Blake, N. R. Champness, P. Hubberstey, D. M. Proserpio, C. Wilson, M. Schröder, *Angew. Chem.* **2004**, *116*, 1887–1890; *Angew. Chem. Int. Ed.* **2004**, *43*, 1851–1854; f) Z. Wang, V. C. Kravtsov, M. J. Zaworotko, *Angew. Chem.* **2005**, *117*, 2937–2940; *Angew. Chem. Int. Ed.* **2005**, *44*, 2877–2880; g) X. M. Zhang, R. Q. Fang, H. S. Wu, *J. Am. Chem. Soc.* **2005**, *127*, 7670–7671; h) X.-L. Wang, C. Qin, E.-B. Wang, Z.-M. Su, *Chem. Eur. J.* **2006**, *12*, 2680–2691.

[6] a) H. Chun, D. Kim, D. N. Dybtsev, K. Kim, *Angew. Chem.* **2004**, *116*, 989–992; *Angew. Chem. Int. Ed.* **2004**, *43*, 971–974; b) R. Natarajan, G. Savitha, P. Dominiak, K. Wozniak, J. N. Moorthy, *Angew. Chem.* **2005**, *117*, 2153–2157; *Angew. Chem. Int. Ed.* **2005**, *44*, 2115–2119; c) M. Du, Z.-H. Zhang, X.-J. Zhao, Q. Xu, *Inorg. Chem.* **2006**, *45*, 5785–5792.

[7] a) V. Niel, A. Galet, A. B. Gaspar, M. C. Muñoz, J. A. Real, *Chem. Commun.* **2003**, 1248–1249; b) B. Yan, C. S. Day, A. Lachgar, *Chem. Commun.* **2004**, 2390–2391, and references therein.

[8] For the three-letter net codes, see ref. [4] and the associated website, http://okeeffe-ws1.la.asu.edu/RCSR/home.htm.

[9] a) S. R. Batten, B. F. Hoskins, B. Moubaraki, K. S. Murray, R. Robson, *J. Chem. Soc. Dalton Trans.* **1999**, 2977–2986; b) S. R. Batten, P. Jensen, B. Moubaraki, K. S. Murray, R. Robson, *Chem. Commun.* **1998**, 439–440; c) C. Qin, X.-L. Wang, E.-B. Wang, Z.-M. Su, *Inorg. Chem.* **2005**, *44*, 7122–7129; d) J. Luo, X. G. Zhou, X. F. Hou, H. X. Wu, L. H. Weng, Y. R. Li, *Chin. J. Chem.* **2005**, *23*, 310–314; e) L. H. Xie, S. X. Liu, B. Gao, C. D. Zhang, C. Y. Sun, D. H. Li, Z. M. Su, *Chem. Commun.* **2005**, 2402–2404; f) C. Qin, X. L. Wang, L. Carlucci, M. L. Tong, E. B. Wang, C. W. Hu, L. Xu, *Chem. Commun.* **2004**, 1876–1877; g) T. Soma, H. Yuge, T. Iwamoto, *Angew. Chem.* **1994**, *106*, 1746–1748; *Angew. Chem. Int. Ed. Engl.* **1994**, *33*, 1665–1666; h) W. Dong, Q.-L. Wang, S.-F. Si, D.-Z. Liao, Z.-H. Jiang, S.-P. Yan, P. Cheng, *Inorg. Chem. Commun.* **2003**, *6*, 873–876; i) T. Soma, T. Iwamoto, *Acta Crystallogr. Sect. C* **1997**, *53*, 1819–1821; j) V. Niel, M. C. Muñoz, A. B. Gaspar, A. Galet, G. Levchenko, J. A. Real, *Chem. Eur. J.* **2002**, *8*, 2446–2453; k) O. Teichert, W. S. Sheldrick, *Z. Anorg. Allg. Chem.* **2000**, *626*, 1509–1513; l) M. Schwarten, J. Chomic, J. Cernak, D. Babel, *Z. Anorg. Allg. Chem.* **1996**, *622*, 1449–1456.

[10] a) J. Kim, B. Chen, T. M. Reineke, H. Li, M. Eddaoudi, D. B. Moler, M. O'Keeffe, O. M. Yaghi, *J. Am. Chem. Soc.* **2001**, *123*, 8239–8247; b) J. H. He, Y. T. Zhang, Q. H. Pan, J. H. Yu, H. Ding, R. R. Xu, *Microporous Mesoporous Mater.* **2006**, *90*, 145–152.

[11] P. Jensen, D. J. Price, S. R. Batten, B. Moubaraki, K. S. Murray, *Chem. Eur. J.* **2000**, *6*, 3186–3195.

[12] S.-Y. Wan, Y.-T. Huang, Y.-Z. Li, W.-Y. Sun, *Microporous Mesoporous Mater.* **2004**, *73*, 101–108.

[13] a) S. R. Batten, B. F. Hoskins, R. Robson, *Angew. Chem.* **1995**, *107*, 884–886; *Angew. Chem. Int. Ed. Engl.* **1995**, *34*, 820–822; b) H. K. Chae, J. Kim, O. D. Friedrichs, M. O'Keeffe, O. M. Yaghi, *Angew. Chem.* **2003**, *115*, 4037–4039; *Angew. Chem. Int. Ed.* **2003**, *42*, 3907–3909; c) E. Y. Lee, S. Y. Jang, M. P. Suh, *J. Am. Chem. Soc.* **2005**, *127*, 6374–6381.

[14] H. K. Chae, D. Y. Siberio-Pérez, J. Kim, Y. Go, M. Eddaoudi, A. J. Matzger, M. O'Keeffe, O. M. Yaghi, *Nature* **2004**, *427*, 523–527.

[15] L. G. Beauvais, M. P. Shores, J. R. Long, *Chem. Mater.* **1998**, *10*, 3783–3786.

[16] D. J. Chesnut, D. Plewak, J. Zubieta, *J. Chem. Soc. Dalton Trans.* **2001**, 2567–2580.

[17] S. C. Xiang, X. T. Wu, J. J. Zhang, R. B. Fu, S. M. Hu, X. D. Zhang, *J. Am. Chem. Soc.* **2005**, *127*, 16352–16353.

[18] B. F. Abrahams, M. G. Haywood, R. Robson, *CrystEngComm* **2005**, *7*, 629–632.

[19] I. A. Baburin, V. A. Blatov, L. Carlucci, G. Ciani, D. M. Proserpio, *J. Solid State Chem.* **2005**, *178*, 2452–2474.

[20] a) S. R. Batten, *CrystEngComm* **2001**, *3*, 67–73; b) http://www.chem.monash.edu.au/staff/sbatten/interpen/index.html.

[21] M. Du, X.-J. Zhao, J.-H. Guo, S. R. Batten, *Chem. Commun.* **2005**, 4836–4838, and references therein.

[22] Bruker AXS, *SAINT Software Reference Manual*, Madison, WI, **1998**.

[23] G. M. Sheldrick, SHELXTL NT (Version 5.1), Program for Solution and Refinement of Crystal Structures, University of Göttingen, Göttingen (Germany), **1997**.

[24] D. C. Palmer, CrystalMaker 7.1.5, CrystalMaker Software, Yarnton, UK, **2006**.

Received: July 8, 2006
Published online: December 22, 2006

